



NURC

a NATO Research Centre
un Centre de Recherche de l'OTAN



PARTNERING
FOR MARITIME
INNOVATION

Reprint Series

NURC-PR-2012-005

The relation between the waveguide invariant, multipath impulse response, and ray cycles

Chris H. Harrison

April 2012

Originally published in:

Journal of the Acoustical Society of America, Vol. 129, No. 5, May 2011,
pp. 2683-2877.

About NURC

Our vision

- To conduct maritime research and develop products in support of NATO's maritime operational and transformational requirements.
- To be the first port of call for NATO's maritime research needs through our own expertise, particularly in the undersea domain, and that of our many partners in research and technology.

One of three research and technology organisations in NATO, NURC conducts maritime research in support of NATO's operational and transformation requirements. Reporting to the Supreme Allied Commander, Transformation and under the guidance of the NATO Conference of National Armaments Directors and the NATO Military Committee, our focus is on the undersea domain and on solutions to maritime security problems.

The Scientific Committee of National Representatives, membership of which is open to all NATO nations, provides scientific guidance to NURC and the Supreme Allied Commander Transformation.

NURC is funded through NATO common funds and respond explicitly to NATO's common requirements. Our plans and operations are extensively and regularly reviewed by outside bodies including peer review of the science and technology, independent national expert oversight, review of proposed deliverables by military user authorities, and independent business process certification.



Copyright © Acoustical Society of America, 2011. NATO member nations have unlimited rights to use, modify, reproduce, release, perform, display or disclose these materials, and to authorize others to do so for government purposes. Any reproductions marked with this legend must also reproduce these markings. All other rights and uses except those permitted by copyright law are reserved by the copyright owner.

NOTE: The NURC Reprint series reprints papers and articles published by NURC authors in the open literature as an effort to widely disseminate NURC products. Users are encouraged to cite the original article where possible.

The relation between the waveguide invariant, multipath impulse response, and ray cycles

Chris H. Harrison^{a)}

NATO Undersea Research Centre, Viale San Bartolomeo 400, 19126 La Spezia, Italy

(Received 22 October 2010; revised 28 January 2011; accepted 17 February 2011)

The waveguide invariant, β , that manifests itself as interference fringes or “striations” in a plot of frequency vs source–receiver separation, is usually thought of as a modal phenomenon. This paper shows that striations can be explained simply through the variation of the eigenray arrival times with range, in short, the variation of the multipath impulse response. It is possible to calculate β for a number of sound speed profiles analytically and to find what β depends on, why it switches from one value to another, how it depends on source–receiver depth, how it depends on variable bathymetry, and how smooth the sound speed profile needs to be for clear fringes. The analytical findings are confirmed by calculating striation patterns numerically starting from eigenray travel times in various stratified environments. Most importantly the approach throws some light on what can be deduced from β alone and the likelihood and utility of striations in reverberation.

© 2011 Acoustical Society of America. [DOI: 10.1121/1.3569701]

PACS number(s): 43.30.Dr, 43.30.Cq [MS]

Pages: 2863–2877

I. INTRODUCTION

The behavior of propagation interference fringes or “striations” as sound source and receiver are separated can be quantified through a “waveguide invariant” called β (Chuprov, 1982; Brekhovskikh and Lysanov, 1991; D’Spain and Kuperman, 1999; Brown *et al.*, 2005). A special case of these striations is the hyperbolic Lloyd mirror fringes that have been used in passive ranging, allowing determination of closest point of approach and ratio of range to source depth (Hudson, 1983; Turgut *et al.*, 2010). More general range localization is discussed by Cockrell and Schmidt (2010) and Sørstrand (2005). In recent years β has been considered as a part of the toolset in geoacoustic inversion (Heaney, 2004) and has been applied to the detection of targets and estimation of reverberation (Goldhahn *et al.*, 2008) and active sonar (Quijano *et al.*, 2008). It has also been tied into topics such as time reversal focusing (Kim *et al.*, 2003), fluctuation statistics (Rouseff, 2002), and beam processing (Yang, 2003). The effects of internal waves on the stability of striation patterns has been studied by Rouseff (2001).

Most of the attempts to understand the patterns have been through the normal modes of the waveguide. A complementary interpretation is that the behavior of the fringes is determined by the behavior of the impulse response as the receiver is moved—this is the approach presented in this paper. Since it is possible to calculate the delay times of eigenrays numerically and in some cases analytically, it is then possible, by writing out their Fourier transform, to see how the fringes will behave. Because thinking in terms of the impulse response is fairly intuitive this approach adds some insight into the more conventional modal method, and in some cases even enables a qualitative solution without detailed computation.

In the high frequency limit the multipath impulse response consists of many positive and negative impulses that correspond to the many eigenrays. The introduction of boundary-reflections, caustics, rough surfaces, low frequencies certainly alters the detailed shape of these impulses, and refraction may alter the sequence but nevertheless the fringe pattern at a given range is the Fourier transform of this impulse response. As the range between the source and receiver changes, the time ordering of the individual impulses generally does not change but their separation does. If the time separations widen, then the fringe separation in frequency reduces in proportion and vice versa.

So one can construct the fringes by numerically calculating eigenray arrival times and rough amplitudes (including signs) using a very crude representation of reflection loss which automatically makes the sequence of impulses to tail off, but with no allowance for caustics, and so on. However, as we will see later, this envelope shape is not important. The fringe pattern is just the modulus-square of the Fourier transform of this impulse response. All the cases illustrated in this paper can be obtained numerically in this manner, but for the sake of credibility more sophisticated models are used in the illustrations, as will be noted later.

The aim of this paper is to investigate the dependence of the interference fringes on range analytically through the quantity “ β ,” the waveguide invariant, which is the slope of $d(\log \omega)/d(\log r)$ or

$$\beta = \frac{d\omega/dr}{\omega/r}. \quad (1)$$

It is well known that $\beta=1$ for isovelocity with reflecting boundaries, and $\beta=-3$ for a uniform sound speed gradient, but there are many other sound speed profiles which are of interest and questions about range dependence, the influence of random sound speed fluctuations, and implications for reverberation.

^{a)}Author to whom correspondence should be addressed. Electronic mail: harrison@nurc.nato.int

Section II explains the reasoning behind the relationship between the eigenray travel times making up the impulse response and the ray cycle distance and cycle time for refracting environments. It discusses about fringes of absolute phase (β) and the more familiar fringes of relative phase (β'), and the effect of source and receiver depth. Section III calculates these parameters for specific sound speed profiles including isovelocity, uniform gradient, linear square of wavenumber, the pathological cosh profile whose β is infinite, parabolic square of wavenumber, and parabolic square of sound speed. A general power law sound speed depth dependence is introduced, which can gradually change from virtually isovelocity with a reflecting boundary, through parabolic, then linear, to square root, and beyond. Section IV considers hybrid profiles with and without reflecting boundaries and shows that some results are almost obvious from a ray point of view. It also shows that randomness in the sound speed profile may eventually destroy any visible stripes in the striation pattern. Section V, in conjunction with the Appendix, distinguishes between the waveguide “invariant” and “ray invariants” and investigates the effect of range-dependent environments on striations. Striations may be observed in reverberation; Sec. VI discusses the implications of the approach of this paper.

II. ANALYSIS

The basic behavior of these fringes and their beta value can be calculated analytically in several cases of interest.

A. Isovelocity

By the method of images it is straightforward to show that the eigenrays arriving at horizontal range r occur at angles θ_n given by

$$\tan \theta_{n,\mu,\nu} = (2nH + \mu z_s + \nu z_r)/r \quad (2)$$

where n is an integer, H is the water depth, $z_{s,r}$ are the source and receiver depths, respectively, and μ, ν both take the values $+1$ and -1 . Travel time is simply

$$t_{n,\mu,\nu} = r \sec \theta_{n,\mu,\nu}/c \quad (3)$$

and the delay after the first return is

$$\tau_{n,\mu,\nu} = \frac{r}{c} (\sec \theta_{n,\mu,\nu} - 1). \quad (4)$$

In the small angle approximation this combined with Eq. (2) becomes

$$\tau_{n,\mu,\nu} = (2nH + \mu z_s + \nu z_r)^2/(2rc). \quad (5)$$

In the eigenray approximation the impulse response consists of a weighted sequence of delta functions at the delays, defined by $\tau_{n,\mu,\nu}$, and consequently the Fourier transform of the impulse response $F(\omega, r)$, whose modulus-square is the fringe pattern, is

$$\begin{aligned} F(\omega, r) &= \int \sum_{\mu,\nu} \sum_n a_n \delta(\tau - \tau_{n,\mu,\nu}) \exp(i\omega\tau) d\tau \\ &= \sum_{\mu,\nu} \sum_n a_n \exp(i\omega\tau_{n,\mu,\nu}). \end{aligned} \quad (6)$$

The summation over μ, ν means that for each value of n in Eq. (2) there are four combinations of μ and ν over which we should also sum. These four terms result in two positive and two negative signs multiplied by almost identical values of the weighting a_n . Thus we can think of Eq. (6) as four separate summations over n in each, of which a_n is a positive slowly varying function of n —in effect an envelope,

$$\begin{aligned} F(\omega, r) &= - \sum_n a_n \exp(i\omega\tau_{n,+1,+1}) - \sum_n a_n \exp(i\omega\tau_{n,-1,-1}) \\ &\quad + \sum_n a_n \exp(i\omega\tau_{n,+1,-1}) + \sum_n a_n \exp(i\omega\tau_{n,-1,+1}). \end{aligned} \quad (7)$$

Substituting Eq. (5) in Eq. (6) for τ_n , and for the moment ignoring the slow variation of a_n we find

$$\begin{aligned} F(\omega, r) &= - \sum_n a_n \exp\left(i(\omega/r)(2nH + z_s + z_r)^2/(2c)\right) \\ &\quad - \sum_n a_n \exp\left(i(\omega/r)(2nH - z_s - z_r)^2/(2c)\right) \\ &\quad + \sum_n a_n \exp\left(i(\omega/r)(2nH + z_s - z_r)^2/(2c)\right) \\ &\quad + \sum_n a_n \exp\left(i(\omega/r)(2nH - z_s + z_r)^2/(2c)\right) \\ &= G(\omega/r). \end{aligned} \quad (8)$$

Thus the complex Fourier transform F is explicitly a function of ω/r , so no matter what its functional form is, it has only one shape as ω and r vary. At any given r there will be a fringe pattern in ω , but moving to a different value of r we find the *same* pattern but stretched in ω in proportion to the increase in r . This automatically constructs a fringe pattern where the modulation takes a constant value along lines where $\omega \propto r$. In other words the condition for a fringe is

$$\frac{\omega}{r} = A = \text{const.} \quad (9)$$

Taking logs and differentiating, we find that this obeys Eq. (1) with $\beta = 1$, as it is well known.

The weights a_n can be written in terms of reflection coefficients, etc.; although since their variation is always much slower than that of the impulses their influence must be small and it does not alter the above argument. It was shown by Harrison and Nielsen (2007) that, for instance, in isovelocity water the one-way multipath pulse envelope decays approximately exponentially with time.

B. General refracting environments

We now extend these ideas to a general refracting environment by attempting to write the Fourier transform in a

form that again demonstrates explicitly the functional dependence on ω and r .

For a general stratified environment the eigenrays for horizontal separation r obey

$$r = nr_c(\theta_{n,\mu,v}) + \mu r_s(\theta_{n,\mu,v}) + \nu r_r(\theta_{n,\mu,v}), \quad (10)$$

where r_c is the cycle distance (double the result of integrating from the top ray turning point to the bottom ray turning point) and r_s and r_r are the partial cycle distances from the top turning point down to the source and receiver depths, respectively. Explicit formulas will be given later. The corresponding eigenray travel times are

$$t_{n,\mu,v}(r) = nt_c(\theta_{n,\mu,v}) + \mu t_s(\theta_{n,\mu,v}) + \nu t_r(\theta_{n,\mu,v}), \quad (11)$$

where the t_c , t_s , and t_r are the full cycle and partial cycle travel times corresponding to r_c , r_s , and r_r .

Equation (7) is true in general but with the behavior of $\tau_{n,\mu,v}$ depending on sound speed profile. So we expect similar relations in Eq. (8) but with the resultant G being a function of the product of ω with some different function of r . As it stands these fringes are in the complex quantity F . Alternatively what is often observed is the modulus-square of F , so the cross terms in $|F|^2$ may be important and these depend on $(t_{n,\mu,v} - t_{m,\mu,v})$. It transpires that the value of β is very slightly different in the two cases (see Appendix A3), and we had estimated both of them below.

C. Condition for a fringe in absolute phase

We need to investigate the delay time $\tau_{n,\mu,v}$ after some range-dependent datum, and we arbitrarily choose range r divided by the minimum sound speed in the profile c_L . So $\tau_{n,\mu,v}$ can be expressed as

$$\begin{aligned} \tau_{n,\mu,v}(r) &= nt_c + \mu t_s + \nu t_r - r/c_L \\ &= n \left(t_c - \frac{r_c}{c_L} \right) + \mu \left(t_s - \frac{r_s}{c_L} \right) + \nu \left(t_r - \frac{r_r}{c_L} \right) \\ &= r \left(\frac{t_c}{r_c} - \frac{1}{c_L} \right) + \mu r_s \left(\frac{t_s}{r_s} - \frac{t_c}{r_c} \right) + \nu r_r \left(\frac{t_r}{r_r} - \frac{t_c}{r_c} \right). \end{aligned} \quad (12)$$

As in the isovelocity case the eigenray impulses still come in groups of four, two positive and two negative, and the separations within a group ($\tau_{n,\pm 1,\pm 1} - \tau_{n,\pm 1,\pm 1}$) are always smaller than the group separation ($\tau_{n+1,\mu,v} - \tau_{n,\mu,v}$) (see Appendix A2). Therefore fringes due to the group separation will be more closely spaced in frequency and more visible than those due to the separation of the members of the group, so we concentrate on group separation. We define the group center as the point $\tau_{n,0,0}$ which is almost identical to the mean of the group.

$$\tau_{n,0,0}(r) = r \left(\frac{t_c(\theta_{n,0,0})}{r_c(\theta_{n,0,0})} - \frac{1}{c_L} \right). \quad (13)$$

The equivalent of Eq. (7) for the groups is

$$\hat{F}(\omega, r) = \sum_n a_n \exp(i\omega \tau_{n,0,0}). \quad (14)$$

As argued earlier [after Eq. (8)], to see fringes it must be possible to write $\tau_{n,0,0}$ as the product of a function of range by only and a function of all the other parameters (e.g., n , H , z_s , etc.). In other words in the exponent of Eq. (14) the range dependence must be separable. This ensures that on going from one range to the next, the Fourier transform \hat{F} may shrink or stretch slightly but always retains its shape. This property forms the striation pattern. Without this property there is no fringe pattern since \hat{F} may vary in an arbitrary manner.

It is always possible to calculate t_c and r_c for a given launch angle (i.e., turning point velocity or horizontal wavenumber). Even if r_c is a discontinuous function of the angle it is still possible to plot $t_c/r_c - 1/c_o$ as a function of cycle distance r_c since the latter is also a function of angle. Thus we can always write τ_n as a function of r_c , say $\tau_n = n(t_c - r_c/c_o) = nG(r_c)$. However this alone (in combination with $r = n \times r_c$) does not ensure that τ_n is a separable function of range r . The only function G that allows separation is $G(r_c) = gr_c^q$ (where g is a proportionality constant), since $G(r_c) = G(r/n) = g r^q \times n^{-q}$. Thus to see fringes (in the complex Fourier transform) we *must* have

$$(t_c - r_c/c_o) r_c^{-q} = g(H, c(z)) = A_j = \text{const} \quad (15)$$

for the j th fringe, and so,

$$\tau_{n,0,0} = n(t_c - r_c/c_o) = r_c^q \times ng = r^q \times n^{1-q} g, \quad (16)$$

where q and g are to be determined and q is a constant. It is shown in Appendix A that by using this equation to evaluate $d(\log \tau_{n,0,0})/d(\log r_c)$, we can evaluate β directly. From Eq. (16) which is the exponent of Eq. (14) then becomes $i\omega r^q \times (n^{1-q} g)$ and for the j th fringe we need

$$\omega r^q = A_j = \text{const}, \quad (17)$$

but taking logs and differentiating we find the behavior exactly as in Eq. (1) with $\beta = -q$. This implies that no other behavior is possible.

D. Condition for a constant relative phase fringe

The relative phase condition depends on $(\tau_{n,\mu,v} - \tau_{m,\mu,v})$, and it is shown in Appendix A that $(\tau_{n,\mu,v} - \tau_{m,\mu,v}) = (n - m)(t_c - r_c K/\omega)$. Following the arguments of the previous section through but starting with $(t_c - r_c K/\omega)$ instead of $(t_c - r_c/c_o)$ we find that Eq. (15) becomes

$$(t_c - r_c K/\omega) r_c^{-q} = g(H, c(z)) = A_j = \text{const} \quad (18)$$

for the j th fringe, and so

$$\begin{aligned} \tau_{n,\mu,v} - \tau_{m,\mu,v} &= (n - m)(t_c - r_c K/\omega) = r_c^q \times (n - m)g \\ &= r^q \times (n - m)^{1-q} g. \end{aligned} \quad (19)$$

Again it is shown in Appendix A that this equation can be used to evaluate β' directly.

E. Source and receiver depth in isovelocity water

From the earlier equations, notably Eq. (8), the source and receiver depths have an effect on the striation pattern itself (i.e., F), as do water depth H and sound speed c . In fact they limit the range of angles (or modes) available to interfere. However the effect on β is weak and non-existent in the isovelocity case as explained in the argument leading to Eq. (9). As noted in Appendix A the source and receiver depths contribute small time offsets around the time $t_{n,0,0}$ that separate the four impulses in each group. These offsets have little effect on the interference fringes and the main pattern is still a function of range.

Writing Eq. (8) another way by combining the source and receiver delays

$$F(\omega, r) = 4 \sum_n a_n \exp(i\omega\tau_{n,0,0}) \sin\left(\omega \int_0^{z_s} \sin\theta/c dz\right) \times \sin\left(\omega \int_0^{z_r} \sin\theta/c dz\right), \quad (20)$$

the sine terms are essentially WKB modes (Wentzel, Kramers, and Brillouin; see [Morse and Feshbach, 1953](#)) that could individually form patterns of horizontal stripes on a plot of frequency vs range, but collectively average to a uniform background for the striations caused by $\tau_{n,0,0}$.

In isovelocity water keeping r and z_s as constant, but varying z_r we see fringes with

$$\omega z_r = A = \text{const}, \quad (21)$$

but these are not as deeply modulated as the fringes in range.

An important different effect of source and receiver depth will be discussed in the context of simultaneously refracting and reflecting environments under ‘‘hybrids’’ in Sec. IV.

III. SPECIFIC SOUND SPEED PROFILES

We can now evaluate t_c , r_c , $\tau_{n,0,0}$ for some given profiles, converting $\tau_{n,0,0}$ to a function of range. We can then evaluate β either through the relation between $\tau_{n,0,0}$ and r or by the following formulas derived in Appendix A. For absolute phase fringes

$$\beta = \frac{1 - \cos\theta}{(c_o t_c / r_c - 1)} = \frac{S_o - S_p}{S_g - S_o} \quad (22)$$

and for relative phase fringes

$$\beta' = \frac{c_o r_c}{(c_o t_c / r_c - \cos\theta)} \bigg/ \left(\omega \frac{dr_c}{dK} \right) = -\frac{\partial S_p}{\partial S_g} = \frac{\sin\theta}{\frac{\partial}{\partial\theta} \left(\frac{c_o t_c}{r_c} \right)}. \quad (23)$$

The latter β' for relative phase fringes corresponds to that calculated by Chuprov and several of the results below can be found in [Chuprov \(1982\)](#). A summary of the results of this section is given in Table I. In all the following examples the ducts are assumed to be one-sided, even though the parabolic and cosh profiles could obviously be extended to two-sided, doubling their cycle distances and times. Figure 1 shows $\log(t_c - r_c/c_o)$ vs $\log r_c$ for each case. The straightness of the

TABLE I. The slope of interference fringes, β , calculated according to Eq. (22) compared with the standard waveguide invariant β' according to Eq. (23) and their approximate forms for various sound speed profiles. For the general profile shape $v = 1 - 1/p$ and $\frac{3-2v}{2v-1} = \frac{v+2}{p-2}$. The asterisks indicate solutions already published by [Chuprov \(1982\)](#).

Sound speed profile	$\beta = -\frac{S_p - S_o}{S_g - S_o} = \frac{1 - \cos\theta}{(c_o t_c / r_c - 1)}$	$\beta' = -\frac{\partial S_p}{\partial S_g} = \sin\theta \bigg/ \frac{\partial}{\partial\theta} \left(\frac{c_o t_c}{r_c} \right)$	Approx.
$c = c_o$	$\cos\theta$	$\cos^2\theta^*$	1
$c(z) = c_o(1 + az)$	$\frac{-3 \cos^2\theta}{1 - 7/10 \tan^2\theta - 3/40 \tan^4\theta \dots}$	$\frac{-3}{1 + 3/5 \sin^2\theta + 3/7 \sin^4\theta \dots}$	-3
$k^2 = k_o^2(1 - az)$	$\frac{-3}{2 - \sec\theta}$	$\frac{-3}{2 - \sec^2\theta}^*$	-3
$c = c_o \cosh az$	∞	∞	∞
$k^2 = k_o^2(1 - a^2 z^2)$	$\frac{2}{\sec\theta - 1} \approx \frac{4}{\theta^2}$	$\frac{2}{\sec^2\theta - 1} = \frac{2}{\tan^2\theta}^*$	$\rightarrow +\infty$
$c^2 = c_o^2(1 + a^2 z^2)$	$\frac{-8 \cos^2\theta (1 + O(\theta^2))}{\tan^2\theta (1 + O(\theta^2))}$	$\frac{-4 \cos^2\theta (1 + O(\theta^2))}{\tan^2\theta (1 + O(\theta^2))}$	$\rightarrow -\infty$
$k^2 = k_o^2(1 - (az)^p)$	$\frac{(3 - 2v)}{2v - (2 - \sec\theta)}$	$\frac{(3 - 2v)}{2v - (2 - \sec^2\theta)}$	$\frac{3 - 2v}{2v - 1}$
$c^2 = c_o^2(1 + (az)^p)$	$\frac{\cos^2\theta(1 + O(\tan^2\theta))}{\frac{2v-1}{3-2v} + O(\tan^2\theta)}$	$\frac{\cos^2\theta(1 + O(\tan^2\theta))}{\frac{2v-1}{3-2v} + O(\tan^2\theta)}$	$\frac{3 - 2v}{2v - 1}$

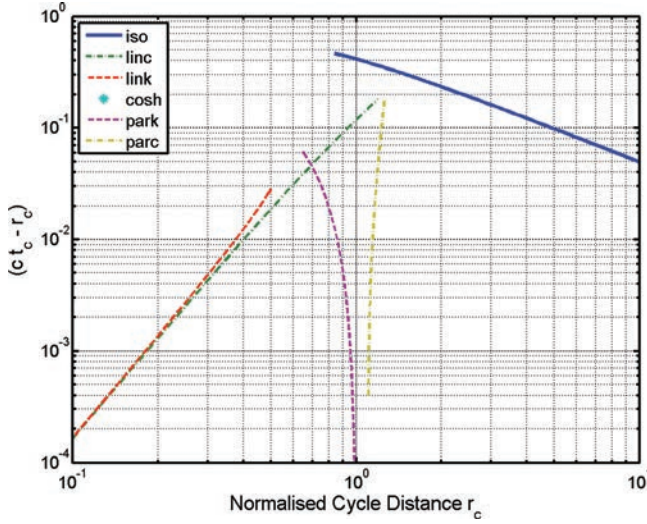


FIG. 1. (Color online) Corrected cycle time $(t_c - r_c/c_o)$ vs cycle distance r_c displayed on a log-log graph for the six profiles labeled as: isovelocity; linear c ; linear k^2 ; cosh; parabolic k^2 ; parabolic c^2 . Gradients correspond to the respective β , so the straight line indicates that β is independent of launch angle.

lines in Fig. 1 shows the goodness of fit to a line of constant β and one can also see the variability between cases.

A. Isovelocity

For an isovelocity profile the cycle time and distance are

$$t_c = 2H/(c \sin \theta) \quad (24)$$

$$r_c = 2H/\tan \theta, \quad (25)$$

whose ratio is $\sec \theta$, so both Eqs. (12) and (13) reduce to

$$\tau_{n,\mu,\nu}(r) = \frac{r}{c} (\sec \theta_{n,\mu,\nu} - 1), \quad (26)$$

as already found in Eq. (4). From Eqs. (22) and (23)

$$\beta = \cos \theta \approx 1 \quad (27)$$

and

$$\beta' = \cos^2 \theta \approx 1. \quad (28)$$

B. Uniform sound speed gradient

Assuming a uniform sound speed gradient with lower speed c_o ,

$$c(z) = c_o(1 + az), \quad (29)$$

the cycle time and distance are

$$\begin{aligned} t_c &= \frac{1}{ac_o} \log \left(\frac{1 + \sin \theta_o}{1 - \sin \theta_o} \right) = \frac{2}{ac_o} \operatorname{atanh}(\sin \theta_o) \\ &= \frac{2}{ac_o} \operatorname{asinh}(\tan \theta_o), \end{aligned} \quad (30)$$

$$r_c = (2/a) \tan \theta_o, \quad (31)$$

where θ_o is measured at the low sound speed boundary. Substituting Eqs. (30) and (31) into Eq. (13) with $c_L = c_o$ we find

$$\begin{aligned} \tau_{n,0,0}(r) &= \frac{r}{c_o} \left(\frac{\operatorname{asinh}(\tan \theta_o)}{\tan \theta_o} - 1 \right) \\ &= -\frac{r}{c_o} \left(\frac{1}{6} \tan^2 \theta_o - \frac{3}{40} \tan^4 \theta_o + \dots \right) \\ &\approx -r^3 \frac{a^2}{24c_o n^2}. \end{aligned} \quad (32)$$

Note that the negative sign is because the chosen arbitrary datum was the slowest speed so that a time advance appears as a negative delay. If instead we had substituted in the complete Eq. (12) there would have been an additional source and receiver term. The source term reduces, after some algebra, to

$$\mu r_s \left(\frac{t_s}{r_s} - \frac{t_c}{r_c} \right) = \mu r_s \left[\left(\frac{1}{c_s} - \frac{1}{c_o} \right) - \frac{a^2 c_o^2}{6} \left(\frac{r_s^2}{c_s^3} - \frac{r_c^2}{c_o^3} \right) \right] \quad (33)$$

and is demonstrably small compared with the rest of Eq. (32). The values of β and β' [Eqs. (22) and (23)] are

$$\beta = \frac{-3 \cos^2 \theta}{1 - 7/10 \tan^2 \theta - 3/40 \tan^4 \theta} \approx -3, \quad (34)$$

$$\beta' = \frac{-3}{1 + 3/5 \sin^2 \theta + 3/7 \sin^4 \theta} \approx -3 \quad (35)$$

and both approximate to the familiar result. Figure 1 shows that the line whose gradient is β is indeed close to being straight.

C. Linear k^2

The profile

$$k^2 = k_o^2(1 - az), \quad (36)$$

i.e.,

$$c^2 = c_o^2/(1 - az) \quad (37)$$

is included here because it is often used in modal analysis. It can be shown that

$$t_c = \frac{4}{ac_o} (\sin \theta_o - \frac{2}{3} \sin^3 \theta_o), \quad (38)$$

$$r_c = (4/a) \cos \theta_o \sin \theta_o \quad (39)$$

and

$$\begin{aligned} \tau_{n,0,0}(r) &= \frac{r}{c_o} (\sec \theta_o - 1 - 2/3 \tan \theta_o \sin \theta_o) \\ &= -\frac{r}{c_o} \left(\frac{\theta_o^2}{6} + \dots \right) \approx -r^3 \frac{a^2}{24c_o n^2}, \end{aligned} \quad (40)$$

$$\beta = \frac{-3}{2 - \sec \theta} \approx -3, \quad (41)$$

$$\beta' = \frac{-3}{2 - \sec^2 \theta} \approx -3, \quad (42)$$

which, to first-order, is the same result as for linear $c(z)$.

D. The cosh profile

It is well known (see Eq. 5.45 of Tolstoy and Clay, 1987) that the profile

$$c = c_o \cosh az \quad (43)$$

leads to perfect focusing with

$$t_c = \frac{\pi}{ac_o} \quad (44)$$

and

$$r_c = \frac{\pi}{a}. \quad (45)$$

Inserting these in Eq. (13) we find $\tau_{n,0,0}=0$ (for all focuses). Thus the sums in Eq. (7) reduce to either no terms or a single term with the exponential term being unity, and so the Fourier transform is either flat in frequency or does not exist. According to Eqs. (22) and (23) both β and β' are infinite. This behavior is demonstrated by the vertical fringes, shown in Fig. 2, calculated with ORCA (Westwood *et al.*, 1996).

Considering a ray trace up to some maximum launch angle [with source on the axis the rays are nearly sine waves, $\sinh(az) = \sinh(az_T) \times \sin(ax)$, where z_T is the

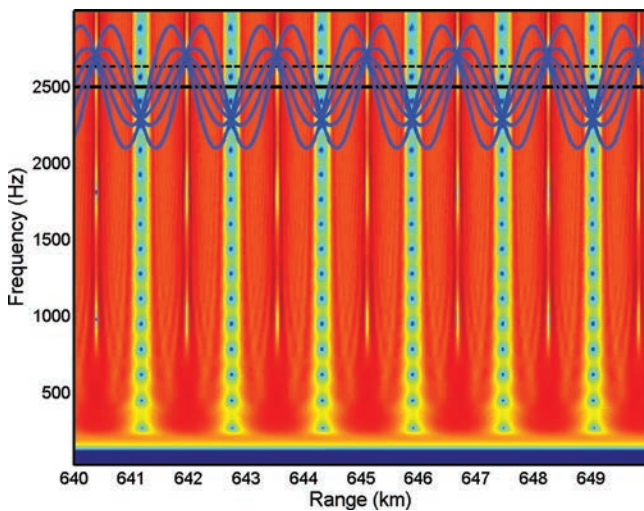


FIG. 2. (Color online) Striations calculated by ORCA for the (two-sided) cosh profile $c = c_o \cosh(az)$. The superimposed and aligned ray trace (receiver depth shown by dashed line) confirms that there may be no arrivals near the focus (when receiver depth is not equal to source complementary depth) and elsewhere only one eigenray, making an exactly repeating pattern once per ray cycle.

turning point depth see Fig. 5.7 of Tolstoy and Clay, 1987] and picking a specific receiver depth we see that for ranges near the focus there are no eigenrays at all (unless the receiver happens to be at the focal depth) and for ranges in between there is only one eigenray. This is confirmed by the ray trace at the top of Fig. 2 (inset). In other words calculation of travel time differences or delays becomes meaningless in this case.

E. Parabolic k^2 (over-curved)

The rather pathological behavior for the cosh profile suggests that a slightly modified profile might be more interesting. The profile $c^2 = c_o^2(1 + a^2z^2)$, though identical to cosh near $z=0$, is slightly less tightly curved elsewhere whereas the profile

$$c^2 = c_o^2/(1 - a^2z^2) \quad (46)$$

is slightly more tightly curved. We take the latter one which can be written in terms of wavenumber $k(z)$ as

$$k^2 = k_o^2(1 - a^2z^2). \quad (47)$$

The tighter curvature means that steep rays curve more than they would in the cosh case and therefore tend to focus at a shorter range. This is reflected in the cycle time and distance which can be shown to be

$$t_c = \frac{\pi}{ac_o}(1 + \cos^2 \theta_o)/2 \quad (48)$$

and

$$r_c = \frac{\pi}{a} \cos \theta_o, \quad (49)$$

where θ_o is measured on the axis, $\cos \theta_o = c(z)/(c_T) = K/k(z)$, c_T is the turning point velocity, and K is the horizontal wavenumber. On substitution into Eq. (13) and defining the axial cycle distance as $r_{c0} = r_c(0)$ such that $r/n = r_c = r_{c0} \cos \theta_o$ we find

$$\begin{aligned} \tau_{n,0,0}(r) &= \frac{r}{c_o} \left(\frac{c_o t_c}{r_c} - 1 \right) = \frac{r}{c_o} \frac{(1 - \cos \theta_o)^2}{2 \cos \theta_o} \\ &= \frac{(nr_{c0} - r)^2}{2c_o nr_{c0}} = \frac{n}{2c_o} \frac{(r_{c0} - r_c)^2}{r_{c0}}. \end{aligned} \quad (50)$$

For each n only certain ranges can contribute impulses because of the limit on θ_o set by the maximum sound speed c_{\max} . These ranges, r , are bounded by nr_{c0} and $nr_{c0} \cos \theta_{\max}$,

$$n > r/r_{c0} > nr_{c0}/c_{\max} \quad (51)$$

and at each range there are limits on n given by

$$n_{\min} = \frac{r}{r_{c0}}; \quad n_{\max} = \frac{rc_{\max}}{r_{c0}c_o}.$$

Equations (22) and (23) give

$$\beta = \frac{2}{\sec \theta - 1} \approx \frac{4}{\theta^2} \rightarrow \infty, \quad (52)$$

$$\beta' = \frac{2}{\sec^2 \theta - 1} \approx \frac{2}{\tan^2 \theta} \rightarrow \infty, \quad (53)$$

which both tend to infinity in the small angle limit.

Although the formula [Eq. (50)] is correct for this profile it is slightly misleading because, as we shall see in Sec. III G, a very slight change in the profile makes a dramatic change in the formula for cycle distance, and this in turn completely alters the behavior of Eq. (50). For now we note that whatever the fringe shape may be they tail off towards range zero, since β is large and positive.

F. Parabolic c^2 (under-curved)

An under-curved version of the cosh curve is

$$c^2 = c_o^2(1 + a^2 z^2). \quad (54)$$

$$\tau_{n,0,0}(r) = \frac{r}{c_o} \frac{(\sec \theta_o - 1 - 1/4 \tan^2 \theta_o (1 + \sec \theta_o) + 3/64 \tan^4 \theta_o (1 + 3 \sec \theta_o))}{(r_c/r_{c0})} \approx -\frac{r}{c_o} \frac{\tan^4 \theta_o}{16 (r_c/r_{c0})}. \quad (57)$$

But from Eq. (56)

$$\frac{\tan^2 \theta_o}{4} \approx \frac{(r_c - r_{c0})}{r_{c0}} \quad (58)$$

so

$$\tau_{n,0,0}(r) \approx -\frac{r}{c_o(r_c/r_{c0})} \left(\frac{r_c - r_{c0}}{r_{c0}} \right)^2 = -\frac{(r - nr_{c0})^2}{c_o nr_{c0}}, \quad (59)$$

where for each n only certain ranges can contribute impulses because of the limit on θ_o set by the maximum sound speed c_{\max} . Thus at each range there are limits on n given by

$$n < r/r_{c0} < n(3 + (c_{\max}/c_o)^2)/4. \quad (60)$$

This is similar behavior to the over-curved parabolic case, but with fringes now tailing off on the far side of the foci. The value of β is

$$\beta = \frac{-8 \cos^2 \theta (1 + 1/4 \tan^2 \theta - 3/64 \tan^4 \theta \dots)}{\tan^2 \theta (1 - \tan^2 \theta + \dots)}. \quad (61)$$

This is a special case of Eq. (82) (Sec. III H) with $\nu = 1/2$. Similarly β' is soluble but messy and can be seen as a special case of Eq. (83) (Sec. III H) with $\nu = 1/2$,

The cycle time and distance integrals are, respectively, elliptic integrals of the first and second kind. When evaluated at the lower limit ($z=0$) they are both zero, and at the upper limit (the ray turning point) they both have their first argument equal to $\pi/2$ and so they are complete elliptic integrals of the first and second kind, and series formulas are given by Abramowitz and Stegun (1972) [Eqs. 17.3.11, 17.3.12].

$$t_c = \frac{2c_T}{ac_o^2} K(-\tan^2 \theta_o) \\ = \frac{\pi}{ac_o} \sec \theta_o (1 - 1/4 \tan^2 \theta_o + 9/64 \tan^4 \theta_o + \dots) \quad (55)$$

and

$$r_c = \frac{2}{a} E(-\tan^2 \theta_o) = \frac{\pi}{a} (1 + 1/4 \tan^2 \theta_o - 3/64 \tan^4 \theta_o + \dots). \quad (56)$$

Again defining the axial cycle distance $r_{c0} = r_c(0) = \pi/a$ we find that now it is longer than for other ray angles. The resulting time separation is

$$\beta' = \frac{-4 \cos^2 \theta (1 + 1/2 \tan^2 \theta - 1/32 \tan^4 \theta \dots)}{\tan^2 \theta (1 - 1/2 \tan^2 \theta + \dots)}. \quad (62)$$

G. General power law $k^2 = k_o^2(1 - (az)^p)$

The cycle time and distance integrals for the profile

$$k^2 = k_o^2(1 - (az)^p) \quad (63)$$

(with $0 < p < \infty$ and $az < 1$ for all z) can be written as

$$t_c = \left(\frac{4k_o^{2\nu-2}}{\omega p a} \right) \int_K^{k_o} \frac{k^3 dk}{\sqrt{k^2 - K^2(k_o^2 - k^2)}^\nu}, \quad (64)$$

$$r_c = \left(\frac{4Kk_o^{2\nu-2}}{p a} \right) \int_K^{k_o} \frac{k dk}{\sqrt{k^2 - K^2(k_o^2 - k^2)}^\nu}, \quad (65)$$

where

$$\nu = 1 - 1/p \quad (66)$$

and K is the horizontal wavenumber. The variety of profiles available is shown in Fig. 3.

These can be solved in terms of the hypergeometric function ${}_2F_1(\alpha, \beta; \gamma; \zeta)$ with fixed values for α, β, γ . However, since the lower integral limit is always a ray turning point (where $k=K$) it vanishes, and the other limit is always

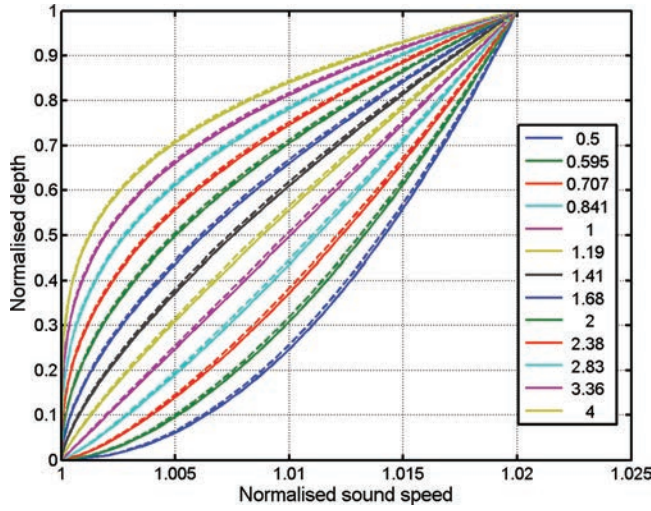


FIG. 3. (Color online) Normalized sound speed profiles $k^2 = k_o^2(1 - (az)^p)$ for various values of the parameter p for which solutions (i.e., t_c , r_c , β) are available.

${}_2F_1(\alpha, \beta; \gamma; 1)$ which simplifies to the ratio of some gamma functions

$${}_2F_1(\alpha, \beta; \gamma; 1) = \frac{\Gamma(\gamma) \Gamma(\gamma - \alpha - \beta)}{\Gamma(\gamma - \alpha) \Gamma(\gamma - \beta)}, \quad (67)$$

the result is

$$t_c = \frac{2\sqrt{\pi} \Gamma(2 - \nu)}{c_o a \Gamma(3/2 - \nu)} \sin^{1-2\nu} \theta_o \left(1 - \frac{(2 - 2\nu)}{(3 - 2\nu)} \sin^2 \theta_o \right), \quad (68)$$

$$r_c = \frac{2\sqrt{\pi} \Gamma(2 - \nu)}{a \Gamma(3/2 - \nu)} \cos \theta_o \sin^{1-2\nu} \theta_o. \quad (69)$$

We can see that these reproduce some of the earlier results, namely linear and parabolic with $p = 1, 2$, ($\nu = 0, 1/2$). In fact the behavior of the isovelocity profile is also reproduced with $p = \infty$, ($\nu = 1$) and $H = 1/a$. In general terms behaviors of cycle time and distance both change over at $p = 2$, ($\nu = 1/2$). For $p > 2$, ($\nu > 1/2$) they decrease from infinity monotonically with angle, whereas for $p < 2$, ($\nu < 1/2$) they increase from zero monotonically with angle.

The time separation in terms of angle is

$$\begin{aligned} \tau_{n,0,0}(r) &= \frac{r}{c_o} \left(\frac{c_o t_c}{r_c} - 1 \right) \\ &= \frac{r}{c_o} \left\{ \sec \theta_o \left(1 - \frac{(2 - 2\nu)}{(3 - 2\nu)} \sin^2 \theta_o \right) - 1 \right\} \\ &\approx \frac{r}{c_o} \left\{ \sin^2 \theta_o \frac{(\nu - 1/2)}{(3 - 2\nu)} + \sin^4 \theta_o \frac{(1 + 2\nu)}{8(3 - 2\nu)} + \dots \right\}. \end{aligned} \quad (70)$$

To write this in terms of r_c we need to substitute for θ_o . Provided ν is not too close to $1/2$ the small angle approximation means that the cosine term in Eq. (69) can be ignored. At exactly $\nu = 1/2$ we see why the solution for the parabolic profile [Eqs. (49) and (50)] was “correct but misleading”; for $\nu < 1/2$ the power of the sine term is posi-

tive and so the cycle distance starts at zero for small angles, whereas for $\nu > 1/2$ the power is negative and the cycle distance starts at infinity. Only at exactly $\nu = 1/2$ is it proportional to cosine. So mathematically we make the approximation

$$\sin \theta_o = \left(\frac{a r_c \Gamma(3/2 - \nu)}{2\sqrt{\pi} \Gamma(2 - \nu)} \right)^{1/(1-2\nu)}, \quad (71)$$

but graphically we can plot the logs of the exact Eq. (70) against the exact Eq. (69) as in Fig. 4. To first order the time separation is

$$\begin{aligned} \tau_{n,0,0}(r) &\approx \frac{n(\nu - 1/2)}{c_o(3 - 2\nu)} \left(\frac{a \Gamma(3/2 - \nu)}{2\sqrt{\pi} \Gamma(2 - \nu)} \right)^{2/(1-2\nu)} r_c^{(3-2\nu)/(1-2\nu)} \\ &\approx \frac{n^{-2/(1-2\nu)}(\nu - 1/2)}{c_o(3 - 2\nu)} \left(\frac{a \Gamma(3/2 - \nu)}{2\sqrt{\pi} \Gamma(2 - \nu)} \right)^{2/(1-2\nu)} \\ &\quad \times r_c^{(3-2\nu)/(1-2\nu)} \end{aligned} \quad (72)$$

Inserting this in Eq. (14) and taking logs, or directly from Eqs. (22) and (23) we find that

$$\beta = \left(\frac{3 - 2\nu}{2\nu - (2 - \sec \theta)} \right) \approx \left(\frac{3 - 2\nu}{2\nu - 1} \right) = \frac{p + 2}{p - 2}, \quad (73)$$

$$\beta' = \left(\frac{3 - 2\nu}{2\nu - (2 - \sec^2 \theta)} \right) \approx \left(\frac{3 - 2\nu}{2\nu - 1} \right) = \frac{p + 2}{p - 2}. \quad (74)$$

The plot in Fig. 4 of the logs of the exact quantities in Eqs. (72) and (69) confirms that these formulas behave well even near $p = 2$. Thus it is possible to find β varying from 1 with large p (quasi-isovelocity) to infinity with $p = 2$ (parabolic), and from minus infinity, through -3 down to -1 with $p = 0$. For p slightly greater than 2, β is large and positive (sloping down toward range zero); for p slightly smaller than 2, β is large and negative (sloping down toward infinite range). Some

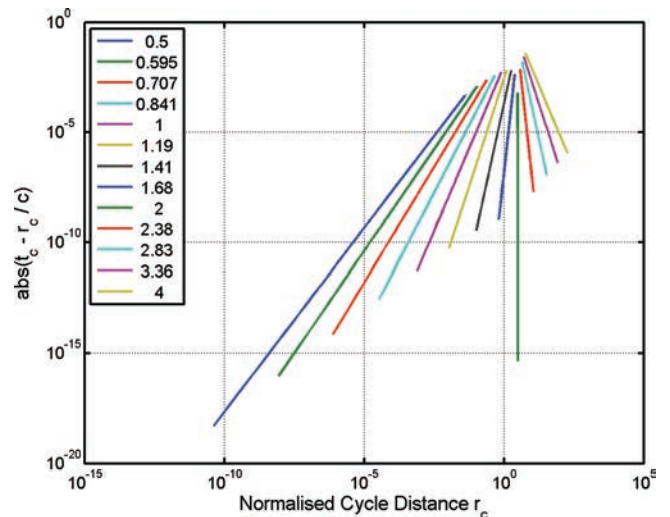


FIG. 4. (Color online) Corrected cycle time vs cycle distance r_c displayed on a log-log graph for various values of the parameter p as shown in Fig. 3. Constant β corresponds to a straight line where $\beta = (p + 2)/(p - 2)$.

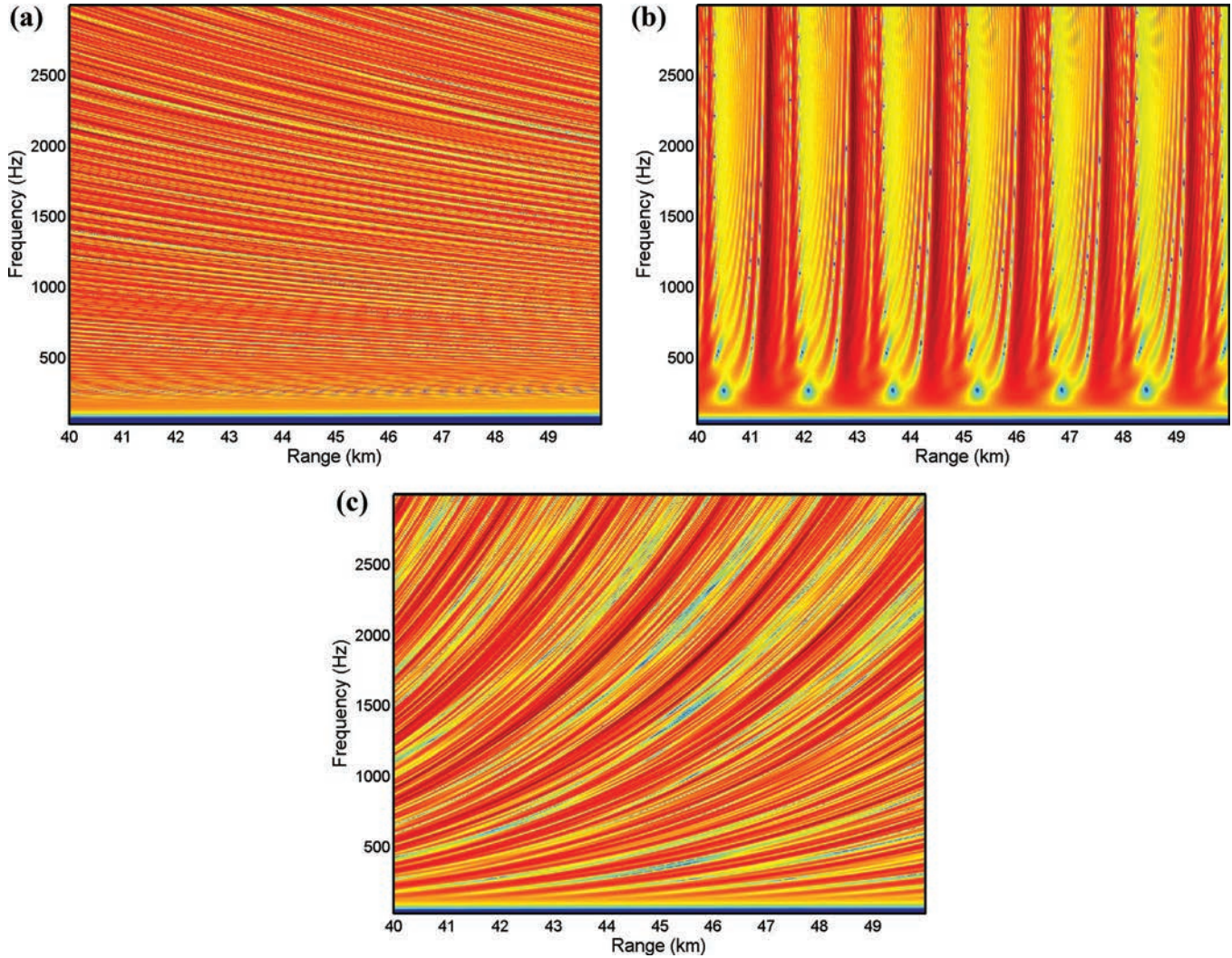


FIG. 5. (Color online) Striations calculated by ORCA for the power law $c^2 = c_o^2/(1 - (az)^p)$. (a) $p=0.5$, (b) $p=2.0$, and (c) $p=2.5$. The fringes follow $\beta = (p + 2)/(p - 2)$ closely.

examples of the striation patterns are shown in Fig. 5 having used ORCA (Westwood *et al.*, 1996). Notice the subtle difference between the $p=2$ case (parabolic) and the cosh case shown in Fig. 2.

H. General power law $c^2 = c_o^2(1 + (az)^p)$

The solutions for the profile

$$c^2 = c_o^2(1 + (az)^p) \tag{75}$$

(with $0 < p < \infty$ and $az < 1$ for all z) can also be written in terms of hypergeometric series. The cycle time and distance integrals can be written as

$$t_c = \left(\frac{4c_T c_o^{2v-2}}{pa} \right) \int_{c_o}^{c_T} \frac{dc}{\sqrt{c_T^2 - c^2} (c^2 - c_o^2)^v}, \tag{76}$$

$$r_c = \left(\frac{4c_o^{2v-2}}{pa} \right) \int_{c_o}^{c_T} \frac{c^2 dc}{\sqrt{c_T^2 - c^2} (c^2 - c_o^2)^v} \tag{77}$$

again with $v = 1 - 1/p$. Now

$$\begin{aligned} t_c &= \frac{2\sqrt{\pi} \Gamma(2-v)}{c_o a \Gamma(3/2-v)} \sec \theta_o \tan^{1-2v} \theta_o \\ &\quad \times {}_2F_1(1-v, 1/2; 3/2-v; -\tan^2 \theta_o) \\ &= \frac{2\sqrt{\pi} \Gamma(2-v)}{c_o a \Gamma(3/2-v)} \sec \theta_o \tan^{1-2v} \theta_o \\ &\quad \times \left(1 - \frac{(1-v)}{(3-2v)} \tan^2 \theta_o + \frac{3(1-v)(2-v)}{2(3-2v)(5-2v)} \tan^4 \theta_o + \dots \right), \end{aligned} \tag{78}$$

$$\begin{aligned} r_c &= \frac{2\sqrt{\pi} \Gamma(2-v)}{a \Gamma(3/2-v)} \tan^{1-2v} \theta_o \\ &\quad \times \left\{ {}_2F_1(1-v, 1/2; 3/2-v; -\tan^2 \theta_o) \right. \\ &\quad \left. + \frac{(1-v)}{(3/2-v)} \tan^2 \theta_o {}_2F_1(2-v, 1/2; 5/2-v; -\tan^2 \theta_o) \right\} \\ &= \frac{2\sqrt{\pi} \Gamma(2-v)}{a \Gamma(3/2-v)} \tan^{1-2v} \theta_o \\ &\quad \times \left(1 + \frac{(1-v)}{(3-2v)} \tan^2 \theta_o - \frac{(1-v)(2-v)}{2(3-2v)(5-2v)} \tan^4 \theta_o + \dots \right). \end{aligned} \tag{79}$$

Again these formulas reproduce results for $p = 1, 2, \infty$, although the $p = 1$ case is not shown in this paper. Note that there is a sudden changeover from the power of the tangent being positive to negative at exactly $v = 1/2$ with a misleading parabolic solution [Eqs. (55) and (56)] in between. The time separation is

$$\begin{aligned} \tau_{n,0,0}(r) &= \frac{n}{c_o} (c_o t_c - r_c) \\ &= \frac{n}{c_o} \left\{ \tan^2 \theta_o \frac{(v - 1/2)}{(3 - 2v)} + O(\tan^4 \theta_o) \right\} \frac{2\sqrt{\pi} \Gamma(2 - v)}{a \Gamma(3/2 - v)} \\ &\quad \times \tan^{1-2v} \theta_o \end{aligned} \quad (80)$$

$$\beta' = \frac{\cos^2 \theta G_2^2}{G_1 G_2 + (1 + t^2)(-2A(G_1 + G_2) + 4Bt^2(G_1 + 3G_2) - 6Ct^4(G_1 + 5G_2))} \quad (83)$$

where

$$t = \tan \theta; \quad A = \frac{1 - v}{3 - 2v}; \quad B = \frac{A}{2} \left(\frac{2 - v}{5 - 2v} \right); \quad C = B \left(\frac{3 - v}{7 - 2v} \right)$$

$$G_1 = 1 - At^2 + 3Bt^4 - 5Ct^6 + \dots$$

$$G_2 = 1 + At^2 - Bt^4 + Ct^6 + \dots$$

Again Eqs. (82) and (83) are approximate to

$$\beta \approx \frac{1}{1 - 4A} = \left(\frac{3 - 2v}{2v - 1} \right) = \frac{p + 2}{p - 2}. \quad (84)$$

as long as $p \neq 2$.

IV. HYBRIDS

A. Bilinear duct

One can construct a sound channel from an upward and a downward linear k^2 duct as in Sec. III C, for example, to make a bilinear duct (see e.g., Eq. 5.42 of Tolstoy and Clay, 1987). However the only effect in this context is that the values of t_c and r_c are doubled. Therefore after substituting in Eq. (13) there is no effect and we find again, $\beta = -3$.

B. Asymmetric ducts

By the same reasoning as above one can construct $\tau_{n,0,0}$ for asymmetric ducts by adding the values of t_c or r_c for the upper and lower parts of the channel. As an example we take Eqs. (30) and (31) and include them in Eq. (32), but now we assume the depth scale a in the upper part and b in the lower part. Note that the components of t_c and r_c are always positive,

$$t_c = \frac{2}{|a|c_o} \operatorname{asinh}(\tan \theta_o) + \frac{2}{|b|c_o} \operatorname{asinh}(\tan \theta_o), \quad (85)$$

and we substitute the first-order expression for r_c as

$$\tan \theta_o = \left(\frac{ar_c \Gamma(3/2 - v)}{2\sqrt{\pi} \Gamma(2 - v)} \right)^{1/(1-2v)}. \quad (81)$$

which, to first-order, leads to the same expression as Eq. (72). Equations (22) and (23) lead to

$$\beta = \frac{\cos^2 \theta (1 + At^2 - Bt^4 + Ct^6 + \dots)}{(1 - 4A) + (8B - 1/2)t^2 + (-12C + B - 1/4A + 3/8)t^4}, \quad (82)$$

$$r_c = \frac{2}{|a|} \tan \theta_o + \frac{2}{|b|} \tan \theta_o. \quad (86)$$

And, surprisingly, this makes absolutely no difference at all to $\tau_{n,0,0}$ and β since the a and b factor out in the ratio of t_c/r_c .

$$\tau_{n,0,0}(r) = \frac{r}{c_o} \left(\frac{\operatorname{asinh}(\tan \theta_o)}{\tan \theta_o} - 1 \right) \approx -r^3 \frac{a^2}{24c_o n^2}. \quad (87)$$

and so beta is still -3 .

C. Combined refraction and reflection

Even with a fixed sound speed profile it is possible for the shape of the fringes to change because at different ranges different parts of the angle or wavenumber range dominate. Figure 6 shows an example with upward refraction where, at short range, boundary-reflected paths dominate leading to $\beta = 1$, but at long range these die out leaving only refracted paths with $\beta = -3$.

Of course, the proportion of refracted rays to reflected rays can also be altered by shifting the source or receiver. Positioning the source and receiver at depths near a low sound speed maximises the number of refracted ray paths; conversely shifting either source or receiver near the maximum sound speed minimises the number of refracted paths. Because the sound speed in the seabed is typically much higher than that in water, the number of reflected paths is not so sensitive to source or receiver depth. Consequently altering receiver depth may make β appear to flip from a reflecting value like $\beta = 1$ to a refracting value like $\beta = -3$. This mechanism may be well responsible for the differences found experimentally by Rouseff (2001) between his Figs. 3(a) and 3(b), where there was a mixed layer down to 12 m and a steep thermocline below. The source was always at a low sound speed at 50 m depth. When the receiver was at 10 m (high sound speed) only reflected paths are effective, leading to $\beta = 1$; when the receiver is at 50 m (low sound speed)

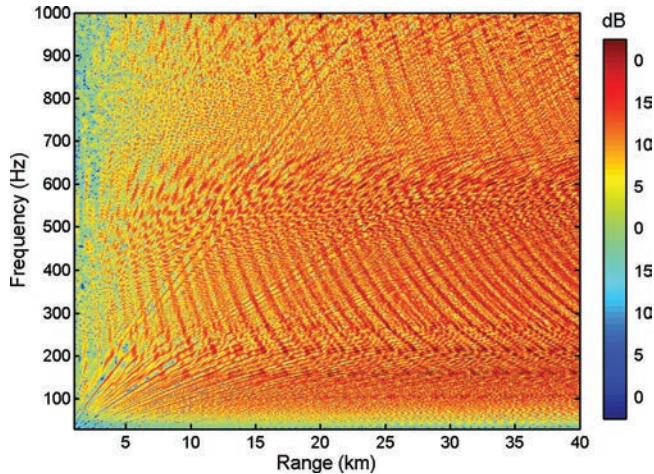


FIG. 6. (Color online) The transition from $\beta = 1$ (at short range) to $\beta = -3$ (at long range) in a range-independent upward refracting environment using ORCA.

there are many competing refracting paths which superimpose fringes with $\beta \sim -3$. This is exactly what Rouseff found experimentally. The interpretation of this author is that his data, like Fig. 6 here, consist of two virtually independent patterns superimposed. This is consistent with Rouseff's interpretation of a distribution of waveguide invariants.

D. Adding variability/randomness

One can take any of the analytical sound speed profiles considered above and numerically calculate the effects of adding some kind of randomness to the profile. From the ray tracing point of view sudden changes in sound speed or its first derivative will result in erratic behavior of the cycle distance and time. From the previous analysis, therefore, one would expect the ensuing chaos to result in an absence of clear fringes. Figure 7 shows that this is indeed what happens. Figure 7(a) is the control result with no randomness; Fig. 7(b) has rather slow variation (the profile is defined by only 21 points) which wipes out the fringes. The corresponding profiles are shown in Fig. 8.

V. RELATIONSHIPS, INVARIANCE, AND RANGE DEPENDENCE

The previous sections investigated the conditions for fringes or striations to form and the dependence of the striation slopes (in frequency-range space) on sound speed profile. No previous theory was invoked and no assumptions were made other than the fringes having a Fourier transform relationship with the eigenray arrival times, i.e. the impulse response. Chuprov's (1985) original meaning of "invariance" was that the quantity β itself was independent of frequency, range, or source/receiver depths in a range-independent environment (Chuprov, 1985, p. 94). All formulas derived here, particularly Eqs. (73) and (74), show this and demonstrate explicit dependence of β on the sound speed profile alone. A number of authors have considered range invariance too (D'Spain and Kuperman, 1999; Brown *et al.*, 2005). So far we have not commented on any range invariant properties

since the environments investigated in this paper were range-independent. Nevertheless the logical starting point that $\omega f(r)$ should be constant for some separable function of range f would still be a valid requirement for a fringe in a range-dependent environment.

To make the connection with range-dependence we use the general relationship derived in the Appendix (Eq. A-2) between cycle time and cycle distance.

$$t_c - r_c K / \omega = (2/\omega) \int \sqrt{k^2 - K^2} dz = 2 \int \sin \theta / cdz. \quad (88)$$

The extreme right hand side is exactly Weston's ray invariant (Weston, 1959) that describes the relation between ray angles and water depth as bathymetry or sound speed change with range. As written in the middle of the equation, the integral is exactly the WKB phase integral (Morse and Feshbach, 1953) which for a bound system, i.e. a reflecting or refracting duct evaluates to $(m + 1/2)\pi$, where m is the mode number. Thus in the adiabatic approximation the mode number itself is an invariant; individual modes do not lose energy to other modes and they stretch and shrink vertically to fit changes in sound speed and bathymetry as they propagate horizontally. Given that the right hand side is definitely an invariant (i.e., a constant for each m or initial ray angle) in a

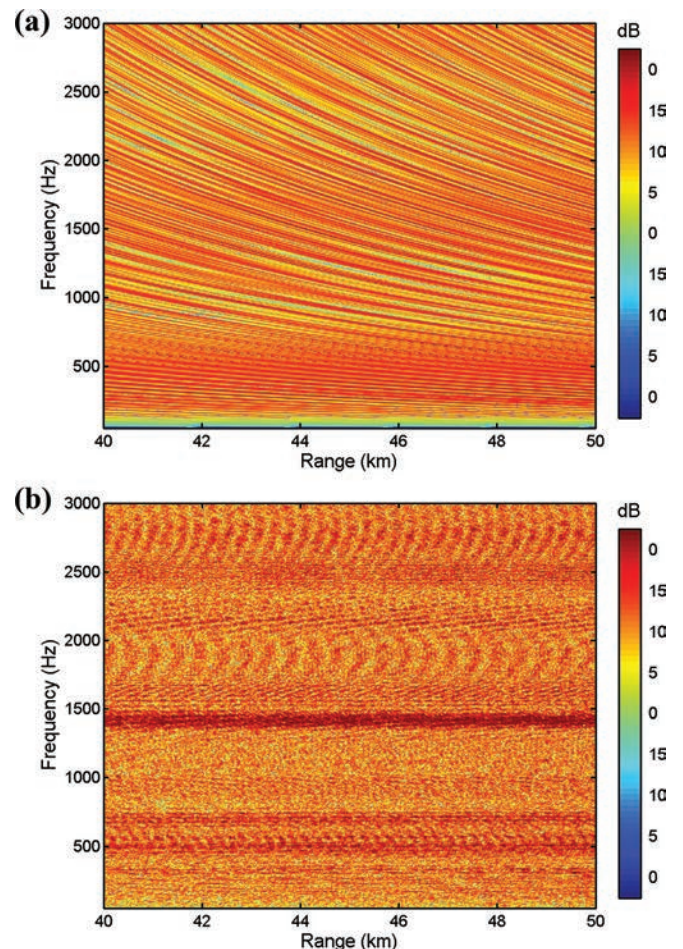


FIG. 7. (Color online) The effect on striations of adding randomness to the sound speed profile (see Fig. 8). (a) pure linear profile and clear fringes; (b) 21 piece-wise linear layers resulting in smudged fringes.

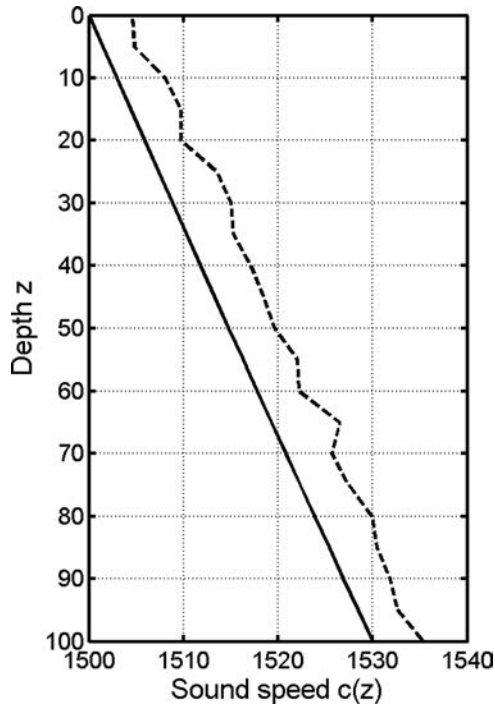


FIG. 8. Sound speed profiles for Fig. 7, pure linear (solid) and 21 piece-wise linear layers (dashed, offset by 5 m/s).

range-dependent environment, we deduce that the left hand side must also be invariant.

Comparing Eq. (88) with (19) we see that the eigenray time difference $(\tau_{n,\mu,v} - \tau_{m,\mu,v})$ which is equal to $(n - m)(t_c - r_c K/\omega)$ must also be invariant with range-dependent environments. However β' is the differential of this quantity with respect to r_c [see Eq. (A-21)] and r_c is not an invariant, and neither is $r_c^2/(dr_c/dK)$ so the outcome is that β' is not generally invariant. Comparing Eq. (16) with Eq. (19) we see that the absolute time $\tau_{n,0,0}$ is also not an invariant.

Nevertheless it is possible to see how the striations will be modified by a change in depth. Harrison and Siderius (2003) showed that the full field, and explicitly the multipath travel times in an (adiabatic) isovelocity range-dependent environment obey

$$t_{n,\mu,v} = r/c + \frac{(2n + \mu z_s/H_s + \nu z_r/H_r)^2}{2c \int_0^r dr/H^2}. \quad (89)$$

Following the argument after Eq. (8) this means that fringes occur when

$$\frac{\omega}{\int_0^r dr/H^2} = A = \text{const.} \quad (90)$$

Thus the otherwise straight fringes (proportional to r) might be skewed by a dip in the seabed, for instance. Figure 9 shows this effect for piece-wise linear bathymetry with five depths of 100, 100, 120, 100, 100 m at 8 km intervals using RAM (Collins, 1993). In Fig. 9(a) this distortion is shown in a plot of ω vs r , and the fringes are clear on both sides of the dip.

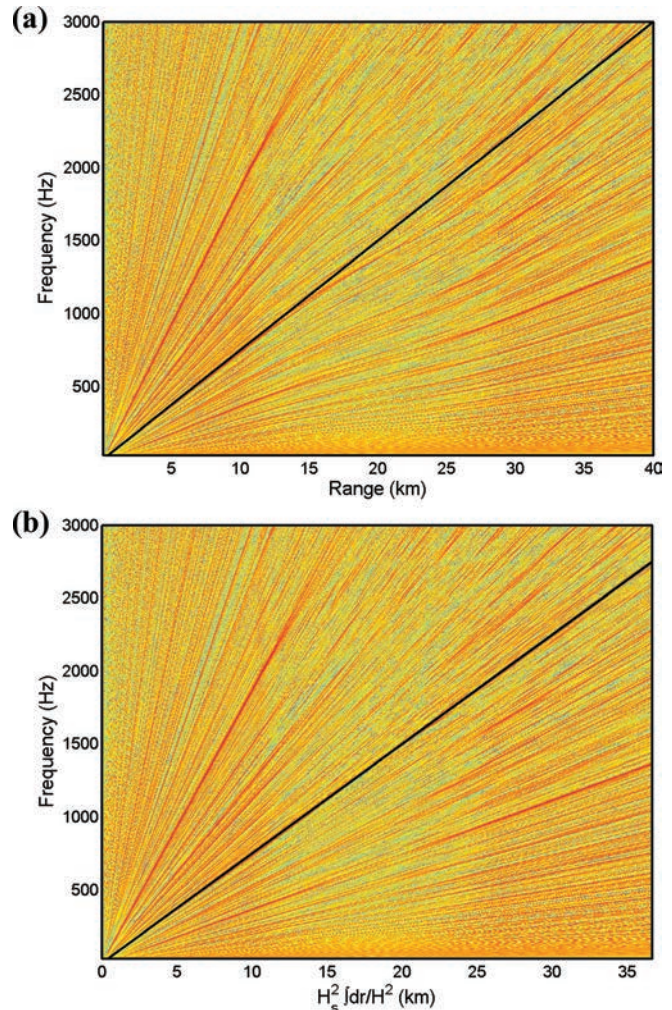


FIG. 9. (Color online) Striations with variable water depth calculated by RAM. Piece-wise linear bathymetry defined by five equally spaced depths (100, 100, 120, 100, 100 m). Plot of frequency against (a) r , and (b) $H_s^2 \int_0^r dr/H^2$. Intensities have been range-corrected to enhance fringe visibility.

One could calculate the integral analytically in this case and superimpose a calculated fringe shape. Instead we choose to plot in Fig. 9(b) ω vs $H_s^2 \int_0^r dr/H^2$ and thus demonstrate the proportionality of Eq. (90) through the straightness of the fringes. The effectiveness of this correction is indeed striking.

VI. SOME IMPLICATIONS FOR REVERBERATION

Reverberation as a function of travel time consists of echoes from scatterers at progressively greater range from source and receiver, so at first sight one would expect striations, being a propagation effect, to appear in the spectrum of broadband reverberation. Experimentally striations are occasionally seen in reverberation, but not always. Some possible reasons are offered by this paper's approach.

- (1) *Source/receiver collocation*: Horizontal separation of source and receiver will cause differences between outward and return propagation fringes which may blur reverberation striations, at least at short range.
- (2) *Smooth sound speed profile*: To see striations the sound speed must be a reasonably smooth function of depth (e.g., continuous second derivative, avoiding real or false

caustics) so that the time separation of the multipath impulses varies smoothly with angle (and therefore cycle distance).

- (3) *Number of eigenrays*: At least a few eigenrays of comparable strength are required to make interference fringes. If either source/receiver or scattering surface is near to the highest sound speed in the duct, the number of eigenrays with refraction turning points will be small leaving only steep rays that interact with both boundaries to form fringes. There is also a scope for differences between the outward and return paths.

VII. CONCLUSIONS

Striation patterns in the propagation spectrum can be thought of as the result of range variation of the multipath impulse response, and so they can be calculated from travel times and therefore ray cycle times and cycle distances. The waveguide invariant β quantifies the range variation of these interference fringes and it has been determined for a number of sound speed profiles including the power law of depth $c^2(z) = c_o^2/(1 - (az)^p)$ and $c^2(z) = c_o^2(1 + (az)^p)$. It was shown that the cosh profile is a pathological case (which is close to a parabolic profile or $p = 2$ in the above formulas) which does not exhibit striation because the exact focusing results in only a single eigenray arrival for all ranges and depths and therefore no interference.

By considering absolute arrival times or time differences it was possible to derive a β for absolute phase and a β' for relative phase in each of the sound speed profile cases. Both can be written in terms of group and phase slownesses, and most of the relative phase formulas are well known.

The approach shows the clear dependence of the waveguide invariant β on path lengths rather than the corresponding eigenray amplitudes. For this reason addition of randomness to the sound speed profile leads to erratic behavior of the cycle time and cycle distance with launch angle, and consequently striation patterns become blurred. Although the propagation spectrum and its interference patterns constitute part of the inputs for geo-acoustic inversion, the value of β by itself is not directly related to seabed properties—even if the seabed is layered.

The distorting effect of variable bathymetry on the fringes was considered. In isovelocity water this distortion can be eliminated by plotting the fringes against frequency and $H_s^2 \int_0^r dr' / H^2$ rather than r itself.

ACKNOWLEDGEMENT

The author thanks Dr. Peter Nielsen for running the examples with ORCA and with RAM.

APPENDIX A: SOME USEFUL RELATIONSHIPS

1. Exact relationships: single eigenray

By considering an element of a ray of length ds at grazing angle θ the horizontal and vertical excursions, dr , dz , and the time increment, dt , are related, for angular frequency ω and local wavenumber $k(z) = \omega/c(z)$, by

$$kds = \omega dt = k \cos \theta dr + k \sin \theta dz. \quad (\text{A1})$$

Integrating in z from one side of the duct to the other ($z = 0$, H), or to a ray turning point, whichever is the sooner, invoking Snell's law, and multiplying by two we find a relation between cycle time t_c and cycle distance r_c

$$\omega t_c - Kr_c = 2 \int_0^H k \sin \theta dz = 2 \int_0^H \sqrt{k^2 - K^2} dz. \quad (\text{A2})$$

Alternatively integrating from the same side down to the source or receiver depth $z_{s,r}$ we have

$$\omega t_{s,r} - Kr_{s,r} = \int_0^{z_{s,r}} k \sin \theta dz = \int_0^{z_{s,r}} \sqrt{k^2 - K^2} dz, \quad (\text{A3})$$

or integrating over the depths of the unwrapped images

$$\begin{aligned} \omega t_n - Kr = 2n \int_0^H \sqrt{k^2 - K^2} dz \pm \int_0^{z_s} \sqrt{k^2 - K^2} dz \\ \pm \int_0^{z_r} \sqrt{k^2 - K^2} dz. \end{aligned} \quad (\text{A4})$$

Differentiating Eq. (A2) with respect to K and noting that the differential of the right hand side is just $-r_c$ we find a relationship between the derivatives of t_c and r_c ,

$$\frac{dt_c}{dK} = \frac{K dr_c}{\omega dK} \quad (\text{A5})$$

and

$$\frac{dt_c}{dr_c} = \frac{K}{\omega}. \quad (\text{A6})$$

Similar relations hold for $t_{s,r}$ and $r_{s,r}$. The quantities t_c and r_c can be calculated through the following integrals across the water column (or at least between ray turning points)

$$t_c = \int 2/(c(z) \sin \theta) dz, \quad (\text{A7})$$

$$r_c = 2 \int \cot \theta dz. \quad (\text{A8})$$

2. Approximate relationships—eigenray pair

The arrival time difference between the m th and n th eigenray ($t_{m,\mu,v} - t_{n,\mu,v}$) is estimated as follows, given that their angular separation is small. Cycle times and cycle distances for m and n are labeled, respectively, with a superscript “+”, “−.” Travel times are

$$t_{m,\mu,v} = t_s^+ + mt_c^+ + t_r^+, \quad (\text{A9})$$

$$t_{n,\mu,v} = t_s^- + nt_c^- + t_r^-. \quad (\text{A10})$$

Horizontal range is

$$r = r_s^+ + mr_c^+ + r_r^+, \quad (\text{A11})$$

$$r = r_s^- + nr_c^- + r_r^- \quad (\text{A12})$$

Assuming that the difference between a “+” and a “-” quantity is accounted for by a slight change in angle $\delta\theta$ (i.e., $t_x^+ = t_x^- + \delta\theta dt_x/d\theta$); we find, by subtracting Eqs. (A10) from (A9)

$$t_{m,\mu,v} - t_{n,\mu,v} = \delta\theta \frac{dt_s}{d\theta} + (m-n)t_c + m\delta\theta \frac{dt_c}{d\theta} + \delta\theta \frac{dt_r}{d\theta} \quad (\text{A13})$$

Subtracting Eqs. (A12) from (A11) we have

$$0 = \delta\theta \frac{dr_s}{d\theta} + (m-n)r_c + m\delta\theta \frac{dr_c}{d\theta} + \delta\theta \frac{dr_r}{d\theta} \quad (\text{A14})$$

Substituting for $\delta\theta$ we find

$$t_{m,\mu,v} - t_{n,\mu,v} = (m-n) \left(t_c + r_c \frac{\frac{dt_s}{d\theta} + m \frac{dt_c}{d\theta} + \frac{dt_r}{d\theta}}{\frac{dr_s}{d\theta} + m \frac{dr_c}{d\theta} + \frac{dr_r}{d\theta}} \right) \quad (\text{A15})$$

and invoking Eq. (A4) this reduces to

$$t_{m,\mu,v} - t_{n,\mu,v} = (m-n)(t_c + r_c K/\omega), \quad (\text{A16})$$

and by Eq. (A2) this is

$$\begin{aligned} t_{m,\mu,v} - t_{n,\mu,v} &= (m-n)(t_c + r_c K/\omega) \\ &= 2(m-n)/\omega \int_0^H \sqrt{k^2 - K^2} dz. \end{aligned} \quad (\text{A17})$$

Using the same method it is easy to show that, for instance,

$$\begin{aligned} t_{n,+1,+1} - t_{n,+1,-1} &= 2(t_r - r_r K/\omega) \\ &= 2/\omega \int_0^{z_r} \sqrt{k^2 - K^2} dz. \end{aligned} \quad (\text{A18})$$

Comparing Eqs. (A17) with (A18) we see that the time separation of groups is always greater than the separation of peaks within a group. For this reason the visible fringes, i.e. those with the closest spacing in frequency, tend to depend on the separation of the groups of four delta functions.

3. Formulas for beta

The quantity β is usually thought of as $d(\log\omega)/d(\log r)$. It was shown in Sec. II that for absolute phase fringes it can be expressed as

$$-\beta = \frac{\partial \log(\tau_{n,0,0})}{\partial \log(r_c)} = \frac{\partial \log(t_c - r_c/c_o)}{\partial \log(r_c)}$$

and for relative phase fringes it is

$$-\beta = \frac{\partial \log(t_{n+1,0,0} - t_{n,0,0})}{\partial \log(r_c)} = \frac{\partial \log(t_c - r_c K/\omega)}{\partial \log(r_c)}$$

Fringes of absolute phase:

$$-\beta = \frac{\partial \log(t_c - r_c/c_o)}{\partial \log(r_c)} = \frac{r_c}{(t_c - r_c/c_o)} \left(\frac{dt_c}{dr_c} - \frac{1}{c_o} \right) \quad (\text{A19})$$

so, with no approximation and making use of Eq. (A6) we have

$$\begin{aligned} \beta &= \frac{-r_c}{(t_c - r_c/c_o)} \left(\frac{K}{\omega} - \frac{1}{c_o} \right) = -\frac{K/\omega - 1/c_o}{(t_c/r_c - 1/c_o)} \\ &= \frac{1 - \cos\theta}{(c_o t_c/r_c - 1)} = \frac{S_o - S_p}{S_g - S_o}. \end{aligned} \quad (\text{A20})$$

where S_g , S_p are group and phase slownesses $S_g = t_c/r_c$, $S_p = K/\omega$, and $S_o = 1/c_o$.

Relative phase fringes:

$$-\beta' = \frac{\partial \log(t_c - r_c K/\omega)}{\partial \log(r_c)} = \frac{-r_c^2}{(\omega t_c - r_c K)} \frac{dr_c}{dK}, \quad (\text{A21})$$

but this can also be written in terms of slownesses using Eq. (A6) since

$$\begin{aligned} -\frac{\partial S_p}{\partial S_g} &= -\frac{\partial(K/\omega)}{\partial(t_c/r_c)} = -\frac{r_c^2}{\omega(r_c dt_c/dK - t_c dr_c/dK)} \\ &= \frac{r_c^2}{(\omega t_c - r_c K)} \frac{dr_c}{dK}, \end{aligned} \quad (\text{A22})$$

so

$$\beta' = -\frac{\partial S_p}{\partial S_g} \quad (\text{A23})$$

as stated by Chuprov (1982) and D'Spain and Kuperman (1999). By substituting Eq. (A2) in the denominator of Eq. (A22) this can be reduced further to

$$\beta' = -\frac{r_c^2}{2 \int_0^H \sqrt{k^2 - K^2} dz} \frac{dr_c}{dK} \quad (\text{A24})$$

as in Brown *et al.* (2005), Eq. (24), and differentiating r_c we have

$$\beta' = -\frac{r_c^2}{2 \int_0^H \sqrt{k^2 - K^2} dz} \frac{\int_0^H \frac{k^2 dz}{(k^2 - K^2)^{3/2}}}{\int_0^H \frac{k^2 dz}{(k^2 - K^2)^{3/2}}}. \quad (\text{A25})$$

Finally for modal propagation the right hand side of Eq. (A2) is twice the WKB phase integral which is related to the mode number m so this can be written as

$$\beta' = -\frac{r_c^2}{2\pi(m + 1/2)} \frac{\int_0^H \frac{k^2 dz}{(k^2 - K_m^2)^{3/2}}}{\int_0^H \frac{k^2 dz}{(k^2 - K_m^2)^{3/2}}}. \quad (\text{A26})$$

Document Data Sheet

<i>Security Classification</i>		<i>Project No.</i>
<i>Document Serial No.</i> NURC-PR-2012-005	<i>Date of Issue</i> April 2012	<i>Total Pages</i> 15 pp.
<i>Author(s)</i> Harrison, C.H.		
<i>Title</i> The relation between the waveguide invariant, multipath impulse response, and ray cycles		
<i>Abstract</i> <p>The waveguide invariant, b, that manifests itself as interference fringes or “striations” in a plot of frequency vs source–receiver separation, is usually thought of as a modal phenomenon. This paper shows that striations can be explained simply through the variation of the eigenray arrival times with range, in short, the variation of the multipath impulse response. It is possible to calculate b for a number of sound speed profiles analytically and to find what b depends on, why it switches from one value to another, how it depends on source–receiver depth, how it depends on variable bathymetry, and how smooth the sound speed profile needs to be for clear fringes. The analytical findings are confirmed by calculating striation patterns numerically starting from eigenray travel times in various stratified environments. Most importantly the approach throws some light on what can be deduced from b alone and the likelihood and utility of striations in reverberation.</p>		
<i>Keywords</i>		
<i>Issuing Organization</i> NURC Viale San Bartolomeo 400, 19126 La Spezia, Italy [From N. America: NURC (New York) APO AE 09613-5000]		Tel: +39 0187 527 361 Fax:+39 0187 527 700 E-mail: library@nurc.nato.int

- Abramowitz, M., and Stegun, I. A. (1972). *Handbook of Mathematical Functions* (Dover, New York), p. 591.
- Brekhovskikh, L. M., and Lysanov, Y. P. (1991). *Fundamentals of Ocean Acoustics*, 2nd ed. (Springer-Verlag, New York), pp. 140–145.
- Brown, M. G., Beron-Vera, F. J., Rypina, I., and Udovychenkov, I. A. (2005). “Rays, modes, wavefield structure, and wavefield stability,” *J. Acoust. Soc. Am.* **117**, 1607–1610.
- Chuprov, S. D. (1982). “Interference structure of a sound field in a layered ocean,” in *Ocean Acoustics, Current Status*, edited by L. M. Brekhovskikh and I. B. Andreyeva (Nauka, Moscow, 1982), pp. 71–91, and (Joint Publications Research Service, Washington DC., 1985), pp. 88–111.
- Cockrell, K. L., and Schmidt, H. (2010). “Robust passive range estimation using the waveguide invariant,” *J. Acoust. Soc. Am.* **127**, 2780–2789.
- Collins, M. D. (1993). “A split-step Padé solution for the parabolic equation method,” *J. Acoust. Soc. Am.* **93**, 1736–1742.
- D’Spain, G. L., and Kuperman, W. A. (1999). “Application of waveguide invariants to analysis of spectrograms from shallow water environments that vary in range and azimuth,” *J. Acoust. Soc. Am.* **106**, 2454–2468.
- Goldhahn, R., Hickman, G., and Krolik, J. (2008). “Waveguide invariant broadband target detection and reverberation estimation,” *J. Acoust. Soc. Am.* **124**, 2841–2851.
- Harrison, C. H., and Siderius, M. (2003). “Effective parameters for matched field geoacoustic inversion in range-dependent environments,” *IEEE J. Ocean. Eng.* **28**, 432–445.
- Harrison, C. H., and Nielsen, P. L. (2007). “Multipath pulse shapes in shallow water: Theory and Simulation,” *J. Acoust. Soc. Am.* **121**, 1362–1373.
- Heaney, K. D. (2004). “Rapid geoacoustic characterization: Applied to range-dependent environments,” *IEEE J. Ocean. Eng.* **29**, 43–50.
- Hudson, R. F. (1983). “A horizontal range vs. depth solution of sound source position under general sound velocity conditions using the Lloyd’s mirror interference pattern,” Master’s thesis, Naval Postgraduate School, Monterey, CA, pp. 1–67.
- Kim, S., Kuperman, W. A., Hodgkiss, W. S., Song, H. C., Edelman, G. F., and Akal, T. (2003). “Robust time reversal focusing in the ocean,” *J. Acoust. Soc. Am.* **114**, 145–157.
- Morse, P. M., and Feshbach, H. (1953). *Methods of Theoretical Physics* (McGraw-Hill, New York), pp. 1098–1099.
- Quijano, J. E., Zurk, L. M., and Rouseff, D. (2008). “Demonstration of the invariance principle for active sonar,” *J. Acoust. Soc. Am.* **123**, 1329–1337.
- Rouseff, D. (2001). “Effects of shallow water internal waves on ocean acoustic striation patterns,” *Waves Random Complex Media* **11**(4), 377–393.
- Rouseff, D. (2002). “Statistics of the waveguide invariant distribution in a random ocean,” in *Impact of Littoral Environment Variability on Acoustic Predictions and Sonar Performance*, edited by N. G. Pace and F. B. Jensen (Kluwer Academic Publishers, Dordrecht), pp. 369–376.
- Søstrand, K. A. (2005). “Range localization of 10–100 km explosions by means of an endfire array and a waveguide invariant,” *IEEE J. Ocean. Eng.* **30**, 207–212.
- Tolstoy, I., and Clay, C. S. (1987). *Ocean Acoustics. Theory and Experiment in Underwater Sound* (AIP, New York), pp. 155–157.
- Turgut, A., Orr, M., and Rouseff, D. (2010). “Broadband source localization using horizontal-beam acoustic intensity striations,” *J. Acoust. Soc. Am.* **127**, 73–83.
- Yang, T. C. (2003). “Beam intensity striations and applications,” *J. Acoust. Soc. Am.* **113**, 1342–1352.
- Weston, D. E. (1959). “Guided propagation in a slowly varying medium,” *Proc. Phys. Soc. London* **73**, 365–384.
- Westwood, E. K., Tindle, C. T., and Chapman, N. R. (1996). “A normal mode model for acousto-elastic ocean environments,” *J. Acoust. Soc. Am.* **100**, 3631–3645.

Document Data Sheet

<i>Security Classification</i>		<i>Project No.</i>
<i>Document Serial No.</i> NURC-PR-2012-005	<i>Date of Issue</i> April 2012	<i>Total Pages</i> 15 pp.
<i>Author(s)</i> Harrison, C.H.		
<i>Title</i> The relation between the waveguide invariant, multipath impulse response, and ray cycles		
<i>Abstract</i> <p>The waveguide invariant, b, that manifests itself as interference fringes or “striations” in a plot of frequency vs source–receiver separation, is usually thought of as a modal phenomenon. This paper shows that striations can be explained simply through the variation of the eigenray arrival times with range, in short, the variation of the multipath impulse response. It is possible to calculate b for a number of sound speed profiles analytically and to find what b depends on, why it switches from one value to another, how it depends on source–receiver depth, how it depends on variable bathymetry, and how smooth the sound speed profile needs to be for clear fringes. The analytical findings are confirmed by calculating striation patterns numerically starting from eigenray travel times in various stratified environments. Most importantly the approach throws some light on what can be deduced from b alone and the likelihood and utility of striations in reverberation.</p>		
<i>Keywords</i>		
<i>Issuing Organization</i> NURC Viale San Bartolomeo 400, 19126 La Spezia, Italy [From N. America: NURC (New York) APO AE 09613-5000]		Tel: +39 0187 527 361 Fax:+39 0187 527 700 E-mail: library@nurc.nato.int